Available online at www.sciencedirect.com
ScienceDirect
Trans. Nonferrous Met. Soc. China 32(2022) 524−539
Transactions of Nonferrous Metals Society of China
www.tnmsc.cn

Formation mechanism and growth kinetics of $TiAl_3$ phase in cold-rolled Ti/Al laminated composites during annealing

Jian-yu ZHANG[1,2], Yan-hui WANG[1,2], Zheng LÜ[1,2], Qing-an CHEN[1,2], Ya-yu CHEN[1,2], He-zong LI[1,2]

1. School of Mechanical and Equipment Engineering, Hebei University of Engineering, Handan 056038, China;
2. Key Laboratory of Intelligent Industrial Equipment Technology of Hebei Province, Hebei University of Engineering, Handan 056038, China

Received 18 January 2021; accepted 10 August 2021

Abstract: Cold-rolled Ti/Al laminated composites were annealed at 525−625 °C for 0−128 h, and the interfacial microstructure evolution was investigated. The results indicate that only the $TiAl_3$ phase was formed at the Ti/Al interface; most of $TiAl_3$ grains were fine equiaxed with average sizes ranging from hundreds of nanometers to several microns and the $TiAl_3$ grain size increased with increasing annealing time and/or temperature, but the effect of annealing temperature on the $TiAl_3$ grain size was far greater than that of annealing time. The growth of the $TiAl_3$ phase consisted of two stages. The initial stage was governed by chemical reaction with a reaction activation energy of 195.75 kJ/mol, and the reaction rate constant of the $TiAl_3$ phase was larger as the Ti/Al interface was bonded with fresh surfaces. At the second stage, the growth was governed by diffusion, the diffusion activation energy was 33.69 kJ/mol, and the diffusion growth rate constant of the $TiAl_3$ phase was mainly determined by the grain boundary diffusion owing to the smaller $TiAl_3$ grain size.

Key words: Ti/Al laminated composites; annealing; growth kinetics; $TiAl_3$ phase; formation mechanism

1 Introduction

Recently, the Ti/$TiAl_3$ metal-intermetallic compound laminated composites have become attractive and potential candidate materials in the fields of aerospace, weapons, and ground military vehicle protection systems due to their excellent properties, such as high yield strength at elevated temperatures, high fracture toughness, high oxidation-corrosion resistance, low density, and good dimension stability [1]. Several technologies based on solid-state reaction between Ti and Al have been developed to fabricate Ti/$TiAl_3$ laminated composites, including diffusion bonding [2], roll bonding with annealing [3,4], explosive welding with annealing [5], and friction stir welding with annealing [6]. By using these methods, only the intermetallic compound $TiAl_3$ phase is usually formed at the Ti/Al interface.

Quite a few studies have focused on the formation mechanism and growth kinetics of the $TiAl_3$ phase during solid-state reaction between Ti and Al. However, the kinetic parameters, such as the kinetic exponent n, growth rate constant K, and activation energy Q, vary widely in different works, and there exist different explanations about the growth mechanism of the $TiAl_3$ phase. For example, LUO and ACOFF [7] investigated the growth kinetics of the $TiAl_3$ phase in Ti/Al laminated composites prepared by cold rolling with subsequent annealing at 650 °C for 0.5−2 h and found that the growth of the $TiAl_3$ phase was dominated by linear law (n=1). KRÁĽ et al [8] studied the growth kinetics of the $TiAl_3$ phase in Ti/Al laminated composites prepared by ion plating

Corresponding author: He-zong LI, Tel: +86-310-3967985, E-mail: lhzong@hebeu.edu.cn
DOI: 10.1016/S1003-6326(22)65813-8

with subsequent annealing at 530−630 °C for 1−20 h and found that the growth of the $TiAl_3$ phase was dominated by parabolic law (n=0.5). FRONCZEK et al [9] found that the growth of the $TiAl_3$ phase in Ti/Al laminated composites prepared by explosive welding with subsequent annealing at 552 °C can be divided into four stages: (1) incubation period (up to 1.5 h), (2) growth governed by chemical reaction for 1.5−5 h (n=1.0), (3) growth governed by volume diffusion for 36−100 h (n=0.48), and (4) growth governed by both chemical reaction and volume diffusion for 5−36 h. However, FOADIAN et al [10] found that the growth of $TiAl_3$ phase in Ti/Al laminated composites prepared by explosive welding with subsequent annealing at 630 °C can only be divided into two stages: (1) growth governed by chemical reaction for 0−12.8 h (n=0.93), and (2) growth governed by grain boundary diffusion for 12.8−260 h (n=0.31). Furthermore, when the kinetic exponent n was equal to 0.5, most studies show that the growth kinetics of the $TiAl_3$ phase was governed by volume diffusion [11−13]. However, some studies [14,15] considered that the growth kinetics of the $TiAl_3$ phase was dominated by mixed diffusion of volume and grain boundary, or even grain boundary diffusion alone. In summary, it can be concluded that the growth kinetics of the $TiAl_3$ phase is still unclear and needs further investigation.

The present work aims to shine new light on the formation mechanism and growth kinetics of the $TiAl_3$ phase. The Ti/Al laminated composites were prepared by cold-rolled bonding. Extensive experimental tests were conducted to study the solid-phase reaction between Ti and Al under different annealing conditions, and the formation mechanism and growth kinetics of the $TiAl_3$ phase were thoroughly studied.

2 Experimental

In this work, the raw materials were commercial Gr.1 pure Ti (99.6 wt.% in purity, and 1 mm in thickness) and pure Al 1050 (99.5 wt.% in purity, and 3 mm in thickness) sheets with dimensions of 200 mm × 300 mm, and the chemical compositions of Ti and Al sheets are shown in Table 1. The Ti sheet was annealed in a vacuum heat treatment furnace at 650 °C for 40 min, and then furnace-cooled to 200 °C and subsequently air-cooled to room temperature. The Al sheet was annealed in a regular heat treatment furnace at 450 °C for 40 min and then air-cooled to room temperature. The annealed Ti and Al sheets were etched by 10 vol.% HF and 10 wt.% NaOH solutions, respectively, cleaned with acetone, and then roughened using steel brush to eliminate surface contamination and prepare a work-hardened layer on the surface for good bonding. The treated Ti and Al sheets were stacked and then bonded by cold rolling with four rolling passes and a 75% total thickness reduction. The as-rolled Ti/Al laminated composites were cut into 10 mm × 15 mm specimens using electro-discharge machining. The specimens were annealed in a regular heat treatment furnace at 525, 550, 575, 600 and 625 °C for different time and then air-cooled to room temperature. The annealing time was 1/12, 1/6, 1/2, 1, 2, 4, 8, 16, 24, 32, 48, 64, 96, and 128 h, respectively.

Table 1 Chemical compositions of Ti and Al sheets (wt.%)

Sample	Fe	C	N	H	O	Others	Ti
Gr.1 Ti	0.20	0.08	0.03	0.015	0.18	0.40	Bal.
Sample	**Si**	**Fe**	**Cu**	**Mn**	**Mg**	**Others**	**Al**
Al 1050	0.25	0.40	0.05	0.05	0.05	0.16	Bal.

The surfaces of all specimens for metallographic examination were on the normal direction (ND)−rolling direction (RD) planes. The cross-sections of all specimens were mechanically ground using SiC abrasive papers (400, 800, and 2000 grit) and polished using diamond powder pastes (2.5 and 0.5 μm). The surface layer of approximately 1 mm in thickness was removed by grinding and polishing to prevent the influence of surface diffusion. The interfacial layer thicknesses were measured by optical microscopy (OM) with image processing software in most specimens and by scanning electron microscopy (SEM) for a small number of specimens. Three specimens were used for each annealing condition, and fifty representative interfacial layer thickness values were measured for each specimen to obtain the average thickness. Because the thickness of the intermetallic compounds at the Ti/Al interface was not uniform, the longer, thicker, and straighter

regions of the interfacial layer were measured as the representative thickness. Some mechanically polished specimens were further electropolished in a solution of $V(HClO_4)$:V(*n*-butanol):V(methanol)= 1:4:5 at −15 °C for 15−20 s under an applied voltage of 27 V, and then the microstructure evolution and chemical compositions of the electropolished specimens were investigated using field-emission scanning electron microscopy (SEM, Zeiss Supra 55) equipped with energy dispersive X-ray spectrometry (EDS) and electron back-scattered diffraction (EBSD) system. The specimens on Al side were dissolved in 10 wt.% NaOH solution, and the rest of the specimens were investigated using X-ray diffractometer (XRD, Bruker D8 Advance) to determine the crystal structure of the intermetallic compounds. Cu K_α radiation was used, the scanning range was 15°−90° and the scan rate was 4 (°)/min.

3 Results and discussion

3.1 Microstructure and phase compositions of Ti/Al laminated composites during annealing

Figure 1(a) shows the back-scattered SEM image of the as-rolled Ti/Al laminated composites. The dark region is identified as Al, the grey region is identified as Ti, and the Ti/Al interface is well bonded with no intermetallic compounds formed. The microstructure evolutions of cold-rolled Ti/Al laminated composites annealed at 525−625 °C are similar. Therefore, Fig. 1 shows only the SEM−EDS images of the cold-rolled Ti/Al laminated composites annealed at 625 °C for different time. After annealing for 5 min, an interfacial layer with an average thickness of 2.01 μm is formed at the Ti/Al interface, as shown in the black-grey region of Fig. 1(b). With increasing annealing time, the average interfacial layer thickness increases continuously. After annealing for 4 h, the average interfacial layer thickness increases to 53.68 μm, as shown in Fig. 1(c). The concentration distribution of Al and Ti in the Ti/Al laminated composites annealed at 625 °C for 4 h is shown in Fig. 1(d). The concentration profiles are almost constant in the intermetallic compound layer, and the molar fractions of Ti and Al are approximately 26.3% and 73.7%, respectively. The molar ratio of Ti to Al is approximate to 1:3, which proves that the intermetallic compound is $TiAl_3$ phase. The Al concentration in the black region is 100% and decreases sharply near the Al/$TiAl_3$ interface, indicating that Ti atoms hardly exist in Al solid solution. Similarly, the Al concentration in the white region is 0 and increases sharply near the

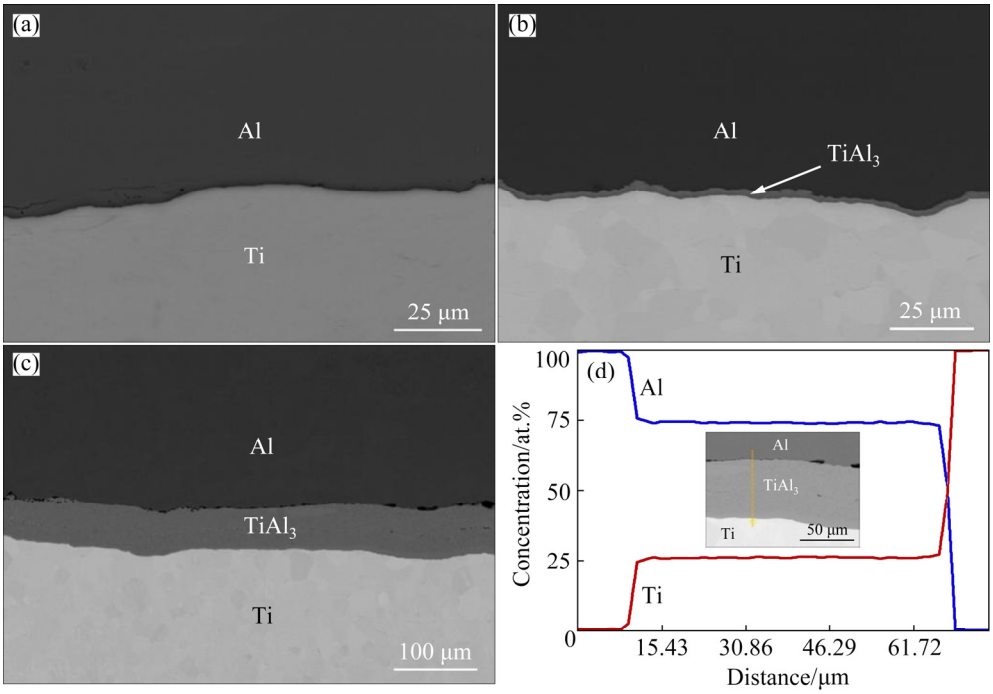

Fig. 1 Back-scattered SEM images of Ti/Al laminated composites: (a) As-rolled; (b) Annealed at 625 °C for 5 min; (c) Annealed at 625 °C for 4 h; (d) Ti and Al concentration profiles of Ti/Al laminated composites annealed at 625 °C for 4 h

$TiAl_3$/Ti interface, indicating that Al atoms hardly exist in Ti solid solution. This could be attributed to the low diffusion coefficients of Al in Ti solid solution and Ti in Al solid solution [16,17], and the low solubility of Ti in Al solid solution [18].

The XRD patterns of the Ti/Al laminated composites annealed at 525, 575, 600 and 625 °C for 64 h are shown in Fig. 2. It can be seen from Figs. 2(a) and (b) that the XRD patterns of the Ti/Al laminated composites annealed at 525 and 575 °C are similar, and from which the $TiAl_3$(l) phase is identified. The $TiAl_3$(l) phase is a low-temperature modification of $TiAl_3$ phase and has a tetragonal crystal structure (Pearson symbol *tI*32, space groups *I*4/*mmm*, lattice parameters $a=b=0.3877$ nm, $c/8=0.4229$ nm, $\alpha=\beta=\gamma=90°$). However, from the diffraction patterns of the Ti/Al laminated composites annealed at 600 and 625 °C (Figs. 2(c) and (d)), a mixture of $TiAl_3$(l) and $TiAl_3$(h) phases is identified. The $TiAl_3$(h) phase is a high-temperature modification of $TiAl_3$ phase and has a tetragonal crystal structure (Pearson symbol *tI*8, space groups *I*4/*mmm*, lattice parameters $a=b=0.3849$ nm, $c/2=0.4305$ nm, $\alpha=\beta=\gamma=90°$). The reason for the existence of $TiAl_3$(h) is that the $TiAl_3$(l)→$TiAl_3$(h) polycrystalline transformation occurs at the annealing temperatures above 600 °C [18−20]. The XRD intensity reveals that the interfacial layer in the Ti/Al laminated composites annealed at 625 °C is mainly $TiAl_3$(h) phase, but both the $TiAl_3$(l) and $TiAl_3$(h) phases occupy a large proportion in the interface layer of the Ti/Al laminated composites annealed at 600 °C.

The EBSD orientation map of the Ti/Al laminated composites annealed at 625 °C for 64 h is shown in Fig. 3, which shows some shadow effects resulting in black non-indexed regions as the electropolishing rate is different for different phases. As shown in Fig. 3, the grain sizes of Ti and Al are very coarse, and there is a tri-modal $TiAl_3$ grain structure between Ti and Al, which consists of Regions *A*, *B* and *C*. Region *A* is located at or near the Ti/$TiAl_3$ interface, in which the $TiAl_3$ phase exhibits fine equiaxed grain structure with an average size of several hundred nanometers. Region *B* is located at the middle of the interfacial layer, in which $TiAl_3$ phase exhibits an equiaxed grain structure with an average size of 1−2 μm. The size

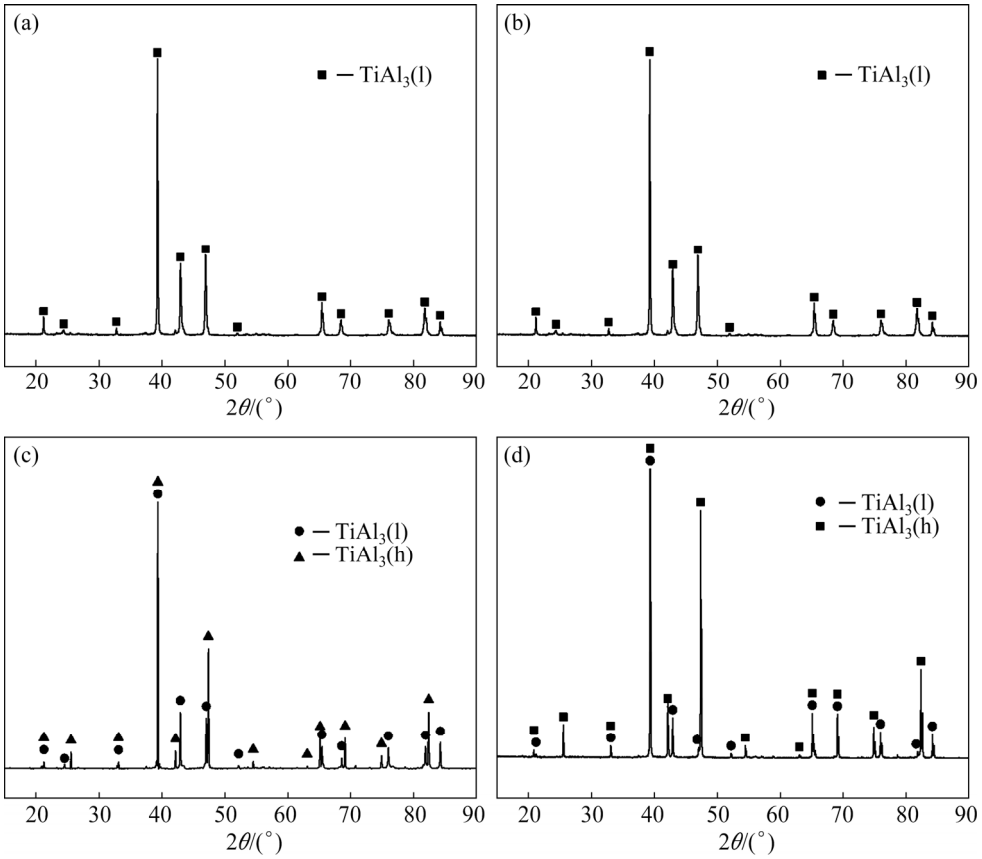

Fig. 2 XRD patterns of cold-rolled Ti/Al laminated composites annealed under different conditions: (a) 525 °C, 64 h; (b) 575 °C, 64 h; (c) 600 °C, 64 h; (d) 625 °C, 64 h

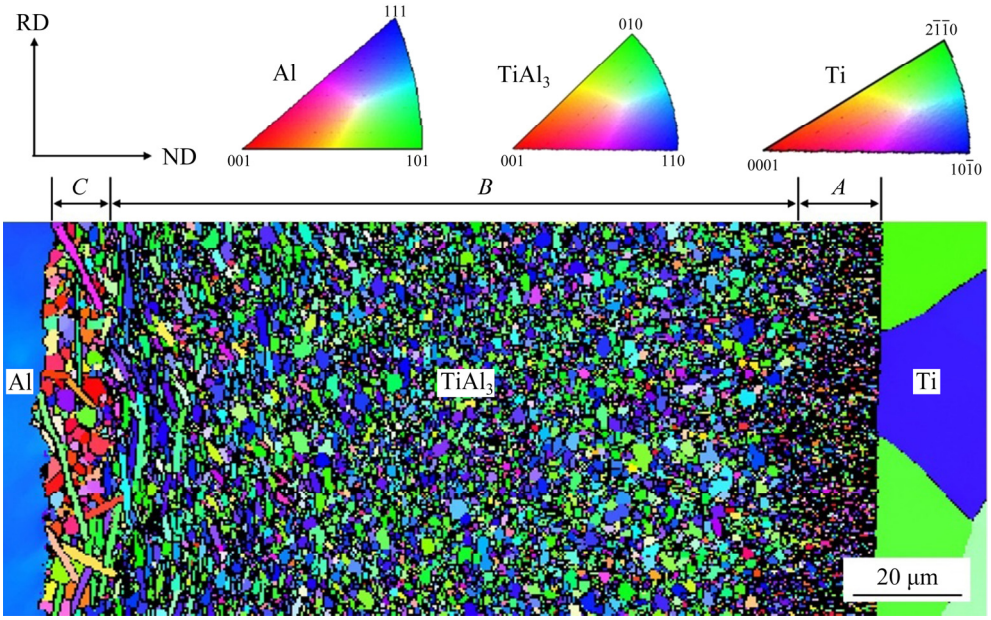

Fig. 3 EBSD orientation map of cold-rolled Ti/Al laminated composites annealed at 625 °C for 64 h

distribution of $TiAl_3$ grains is uniform in most areas of Region *B* except that some $TiAl_3$ grains near the Al side are columnar. Region *C* is located at or near the Al/$TiAl_3$ interface, in which most of the $TiAl_3$ particles exhibit coarse equiaxed grains with an average size of 3−4 μm, and a small part of the $TiAl_3$ particles exhibit columnar grains. In addition, the $TiAl_3$ grain orientation in Region *C* is different from that in Region *B*. The tri-modal $TiAl_3$ grain structure in this experiment is like that in the experiments of THIYANESHWARAN et al [21]. The results in Ref. [21] show that Region *A* consists of the newly fine $TiAl_3$ grains formed at the Ti/$TiAl_3$ interface; Region *B* consists of the already present $TiAl_3$ grains which shift towards the Al side due to the growth of new $TiAl_3$ grains at or near the Ti/$TiAl_3$ interface, and the closer the $TiAl_3$ grains are to the Al side, the longer the annealing time is; Region *C* consists of the $TiAl_3$ grains formed at the Al/$TiAl_3$ interface.

Figure 4 shows the EBSD orientation maps of the central region of the interfacial layer in cold-rolled Ti/Al laminated composites annealed under different conditions. In Fig. 4, the $TiAl_3$ grains on the lower side of the EBSD orientation maps are closer to the Ti/$TiAl_3$ interface than those on the upper side. After annealing at 625 °C for 4 h (Fig. 4(a)), the size of most $TiAl_3$ grains in the EBSD orientation map of the central region is 1−2 μm, while the size of a small amount of $TiAl_3$ grains increases to 3−4 μm. After annealing at 625 °C for 32 and 128 h (Figs. 4(b) and (c)), the size of $TiAl_3$ grains increases slightly with increasing annealing time. After annealing at 575 °C for 32 h (Fig. 4(d)), the size of most $TiAl_3$ grains is several hundreds of nanometers, and the size of a small amount of $TiAl_3$ grains is 1−2 μm. After annealing at 575 °C for 128 h (Fig. 4(e)), the size of $TiAl_3$ grains increases slightly compared with that of the $TiAl_3$ grains annealed at 575 °C for 32 h. As shown in Fig. 4(f), the size of the $TiAl_3$ grains annealed at 525 °C for 128 h is smaller than that annealed at 575 °C for 128 h, whilst the size of almost all $TiAl_3$ grains is below 500 nm. In general, the grain size of $TiAl_3$ phase increases with the increase of annealing temperature and the prolongation of annealing time, but compared with the annealing temperature, the effect of annealing time on the $TiAl_3$ grain size is smaller.

3.2 Growth kinetics of $TiAl_3$ layer at Ti/Al interface

The average thicknesses of the $TiAl_3$ layer in the Ti/Al laminated composites annealed at 525−625 °C for different time are shown in Table 2. The $TiAl_3$ layer thicknesses increase with increasing annealing time at different annealing temperatures. In the temperature range of 525−600 °C, the $TiAl_3$ layer thickness increases with increasing annealing temperature for the same annealing time. However,

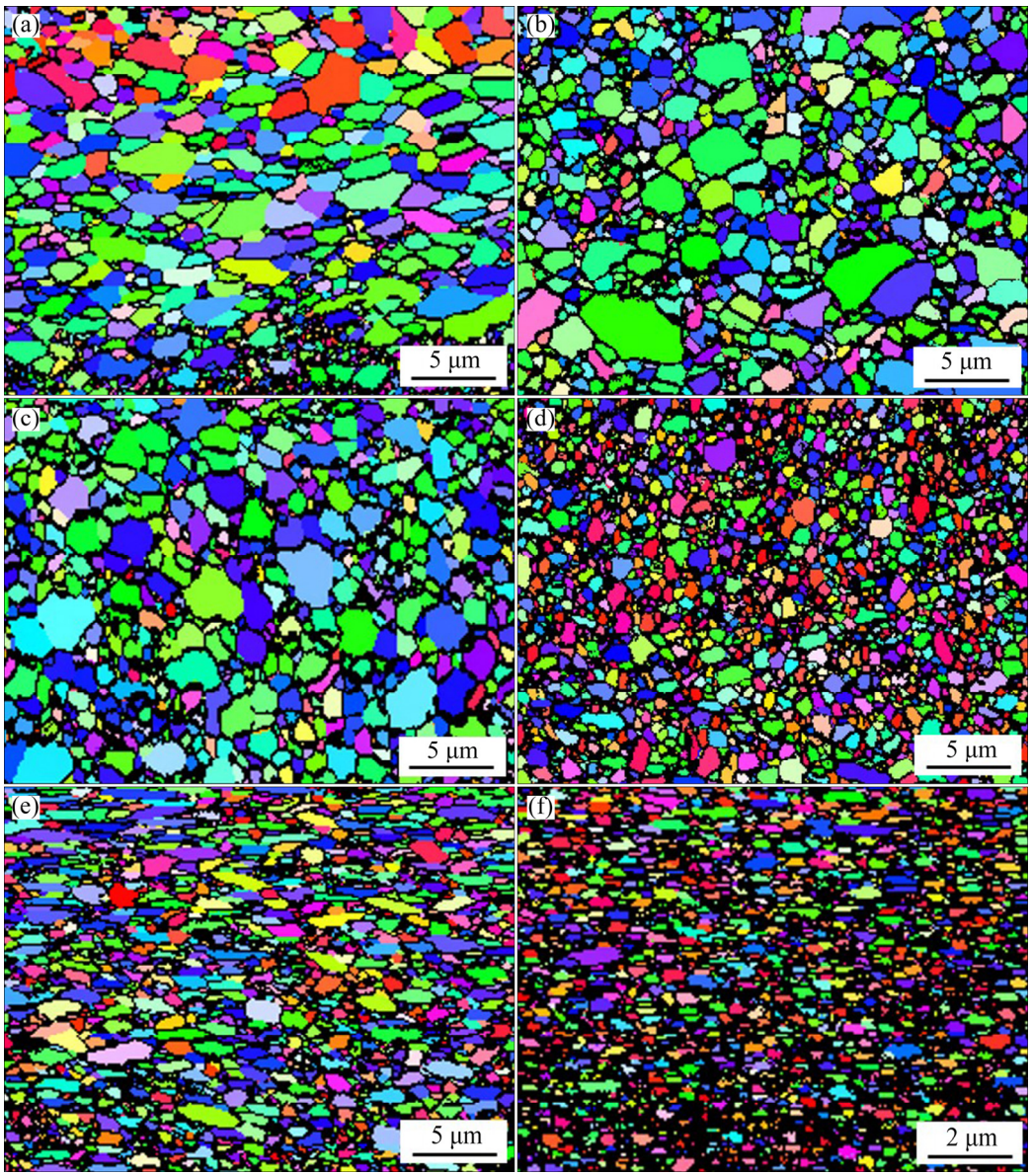

Fig. 4 EBSD orientation maps of central region of interfacial layer in cold-rolled Ti/Al laminated composites annealed under different conditions: (a) 625 °C, 4 h; (b) 625 °C, 32 h; (c) 625 °C, 128 h; (d) 575 °C, 32 h; (e) 575 °C, 128 h; (f) 525 °C, 128 h

in the time range of 8−128 h at 625 °C, the $TiAl_3$ layer thicknesses are even slightly smaller than those annealed at 600 °C for the same annealing time.

At a given temperature, the annealing time-dependent $TiAl_3$ layer thickness (x) can be described by the following empirical relationship [22]:

$$x^{1/n}=K(t-t_0) \quad (1)$$

where K is the rate constant, t is the annealing time, t_0 is the incubation time, and n is the kinetic exponent. There are four possible values for n: 1, 0.5−1, 0.5 and <0.5. The first value is for the growth governed by chemical reaction, the second value is for the growth governed by the combination of chemical reaction and diffusion, the third value is for the growth governed by volume diffusion or the combination of volume diffusion and grain boundary diffusion with grain size remaining unchanged, and the last value is for the growth governed by the combination of volume diffusion and grain boundary diffusion with grain size increasing [23].

Because the $TiAl_3$ phase nucleates rapidly at the Ti/Al interface during annealing at 525−625 °C (see Fig. 1(b)), the incubation time t_0 can be set to

Table 2 Experimental data of average thickness of $TiAl_3$ interfacial layer under different annealing conditions

Time/h	$TiAl_3$ layer thickness/μm				
	525 °C	550 °C	575 °C	600 °C	625 °C
1/12	−	−	−	−	2.01
1/6	−	−	−	2.31	3.97
1/2	−	−	−	6.88	13.29
1	−	2.32	3.80	14.75	22.83
2	1.46	5.39	10.32	23.23	33.53
4	2.75	11.56	18.12	46.03	53.68
8	5.76	24.05	33.15	72.09	71.86
16	10.52	46.84	70.33	97.40	99.27
24	16.32	66.64	82.21	118.02	119.21
32	25.06	81.93	99.22	130.48	132.04
48	41.62	100.44	133.92	150.06	147.99
64	53.14	125.83	156.04	177.04	172.39
96	76.75	154.48	187.91	204.97	203.39
128	96.15	191.24	214.84	227.88	220.05

be zero. The double logarithmic curves of the $TiAl_3$ layer thickness versus annealing time are shown in Fig. 5. Linear regression analysis shows that n=1.04 at 525 °C in the time period of 0−128 h (Fig. 5(a)), which proves that this process is mainly governed by chemical reaction. However, the growth of the $TiAl_3$ layer can be divided into two stages at other annealing temperatures. At the first stage, the values of n are determined as 1.03, 1.01, 0.93 and 1.01 for the time periods of 0−32, 0−16, 0−4 and 0−1 h at 550, 575, 600 and 625 °C, respectively (Fig.5(a)), which indicates that these processes are mainly governed by chemical reaction. At the second stage, the values of n are determined as 0.61, 0.56, 0.45 and 0.46 for the time periods of 32−128, 16−128, 4−128 and 1−128 h at 550, 575, 600 and 625 °C, respectively (Fig. 5(b)), which proves that these processes are mainly governed by diffusion. For the sake of simplicity, the transitional stages from the chemical reaction-controlled growth to the diffusion-controlled growth at different temperatures are neglected. The thickness corresponding to the transition from the chemical reaction growth stage to the diffusion growth stage can be defined as the critical thickness x_{Cr}. As shown in Fig. 5, the values of x_{Cr} are found to be 81.93, 70.33, 46.03 and 22.83 μm at 550, 575, 600 and 625 °C, respectively. Due to the large time interval between different measurement values, the values of x_{Cr} obtained from Fig. 5 are only approximately to the actual critical thickness values. The critical thickness decreases with increasing annealing temperature, which is consistent with the results in Ref. [24].

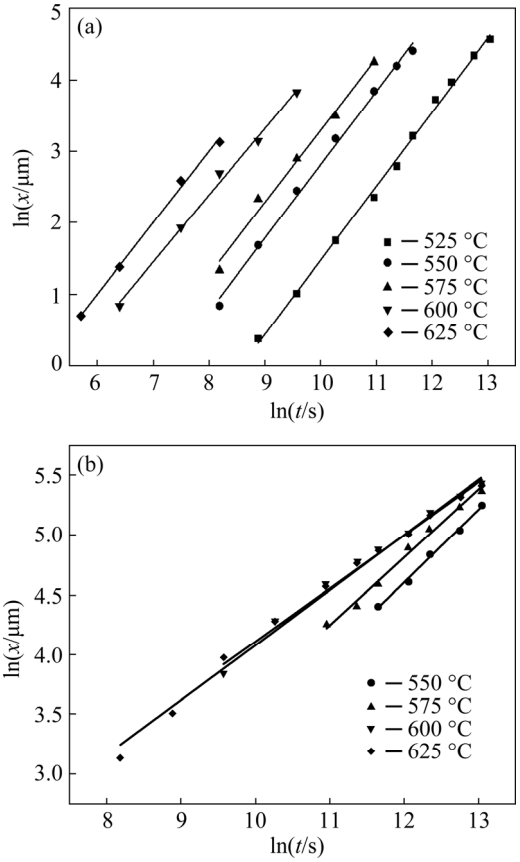

Fig. 5 Plots of $\ln x$ versus $\ln t$ at different annealing temperatures: (a) At reaction-controlled growth stage; (b) At diffusion-controlled growth stage

It should be noted that at the diffusion-controlled growth stage, the deviation of the n value from 0.5 at 550 and 575 °C is greater than that at 600 and 625 °C. This can be attributed to the fact that the time to form the critical thickness x_{Cr} for the chemical reaction-controlled growth is different from that for the diffusion-controlled growth, as shown in Fig. 6 (the dashed line represents a hypothetical diffusion-controlled growth). Hence, when Eq. (1) is used to calculate the value of n for the diffusion-controlled growth, a deviation will be prone to occur if the time period of the chemical reaction-controlled stage takes a larger proportion of the total annealing time. If it is assumed that the time difference between the chemical reaction-controlled growth and the diffusion-controlled growth to form the same critical thickness x_{Cr} is the

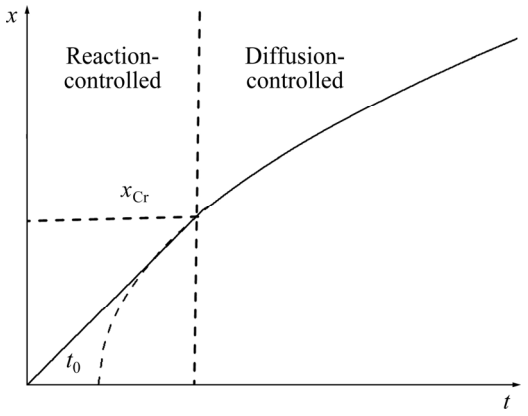

Fig. 6 Parabolic growth plot showing transition from chemical reaction-controlled growth to diffusion-controlled growth

hypothetical incubation time of diffusion-controlled growth, based on Eq. (1), the incubation time t_0 can be calculated by the following equation:

$$t_0=t_1-\frac{x_1^2(t_2-t_1)}{x_2^2-x_1^2} \tag{2}$$

where x_1 and x_2 are the $TiAl_3$ layer thicknesses at annealing time t_1 and t_2, respectively. To calculate the value of t_0 at 550 °C, the value of t_1 is set to be 32 h, and t_2 is set to be 64, 96 and 128 h, respectively. To calculate the value of t_0 at 575 °C, the value of t_1 is set to be 16 h, and t_2 is set to be 48, 64, 96 and 128 h, respectively. Using Eq. (2), the average values of t_0 are determined to be 8.6 and 3.3 h for 550 and 575 °C, respectively. If the incubation time t_0 is considered at 550 and 575 °C, the values of n at the diffusion-controlled growth stage are determined to be 0.52 and 0.51 for 550 and 575 °C, respectively. The reason why the calculated values of n are less than 0.5 at 600 and 625 °C may be that the $TiAl_3$ grains grow slowly with annealing time. If the data in the time period of 0−64 h are used, the values of n are calculated as 0.47 and 0.48 for temperatures from 600 to 650 °C, respectively, which are closer to 0.5.

At the chemical reaction-controlled growth stage, the relationship between the thickness of the $TiAl_3$ layer and annealing time is shown in Fig. 7(a). Through linear regression analysis, the chemical reaction rate constants K_c are determined to be 2.17×10^{-10}, 7.29×10^{-10}, 1.21×10^{-9}, 3.10×10^{-9} and 6.36×10^{-9} m/s at 525, 550, 575, 600 and 625 °C, respectively. At the diffusion-controlled growth stage, the relationship between the square of the

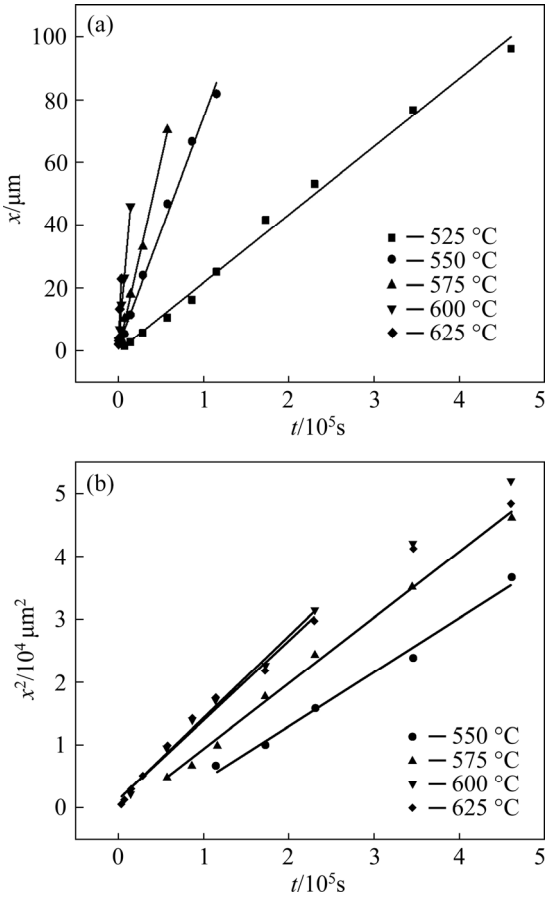

Fig. 7 Relationships of $TiAl_3$ layer thickness and annealing time at different annealing temperatures: (a) At chemical reaction-controlled growth stage; (b) At diffusion-controlled growth stage

$TiAl_3$ layer thickness and annealing time is shown in Fig. 7(b). By using linear regression analysis, the diffusion growth rate constants K_d are determined to be 8.58×10^{-14}, 1.05×10^{-13}, 1.29×10^{-13} and 1.26×10^{-13} m^2/s at 550, 575, 600 and 625 °C, respectively. Here, only the $TiAl_3$ layer thicknesses in the time period of 0−64 h are used for 600 and 625 °C, respectively. Both K_c and K_d obey the Arrhenius formula as follows [23]:

$$K_c=K_{c0}\exp[-Q_c/(RT)] \tag{3}$$

$$K_d=K_{d0}\exp[-Q_d/(RT)] \tag{4}$$

where K_{c0} and K_{d0} are the pre-exponential factors for the chemical reaction-controlled growth and the diffusion-controlled growth, respectively; Q_c and Q_d are the activation energies for the chemical reaction-controlled growth and the diffusion-controlled growth, respectively; R is the gas constant, and R= 8.314 J/(mol·K); T is the thermodynamic temperature. The values of K_{c0}, K_{d0}, Q_c and Q_d can be obtained by

the plots of ln K_c and ln K_d versus the reciprocal of temperature $1/T$ for the $TiAl_3$ layer growth, as shown in Fig. 8. Through linear regression analysis, the values of K_{c0} and Q_c are determined to be 1.57×10^3 m/s and 195.75 kJ/mol, respectively (Fig. 8(a)). The values of K_{d0} and Q_d are determined to be 1.22×10^{-11} m^2/s and 33.69 kJ/mol, respectively (Fig. 8(b)).

3.3 $TiAl_3$ phase formation mechanism in cold-rolled laminated composites during annealing

According to the Ti−Al binary alloy phase diagram in Fig. 9(a) [20], when the Ti/Al diffusion couples are annealed in the temperature range of 525−625 °C, four intermetallic compounds, Ti_3Al, TiAl, $TiAl_2$ and $TiAl_3$, should be formed theoretically. However, it is found that only the $TiAl_3$ phase was formed at the Ti/Al interface in the present work. The absence of other phases is determined by both thermodynamic and kinetic factors. Compared with other Ti−Al intermetallic compounds, the $TiAl_3$ phase nucleates firstly at the Ti/Al interface due to its lowest effective formation heat [22] and lowest interfacial energy increase [25]. In addition, because the interdiffusion coefficient of the $TiAl_3$ phase is much larger than those of other Ti−Al intermetallic compounds, the growth of the latter is suppressed. Therefore, other intermetallic

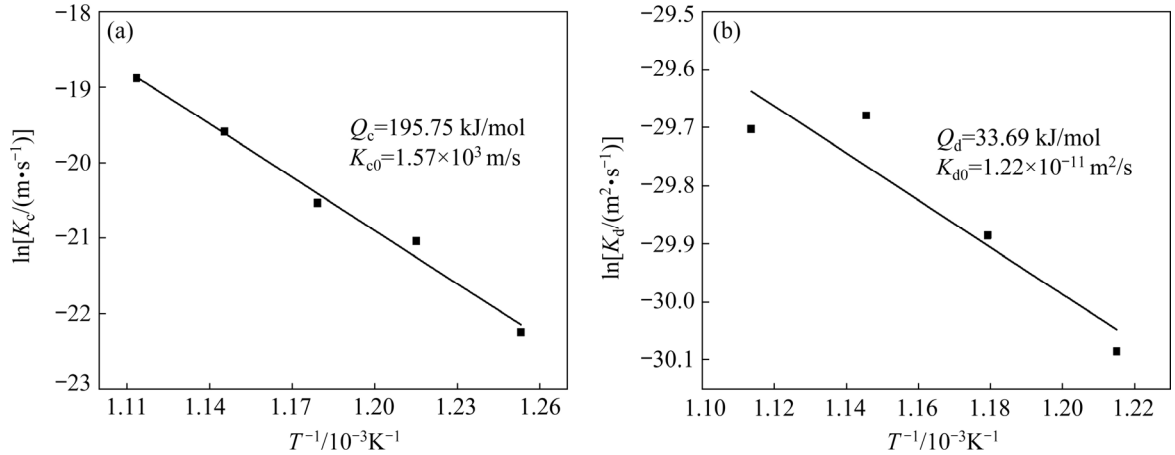

Fig. 8 Plot of ln K_c versus T^{-1} for $TiAl_3$ layer at chemical reaction-controlled growth stage and plot of ln K_d versus T^{-1} for $TiAl_3$ layer at diffusion-controlled growth stage

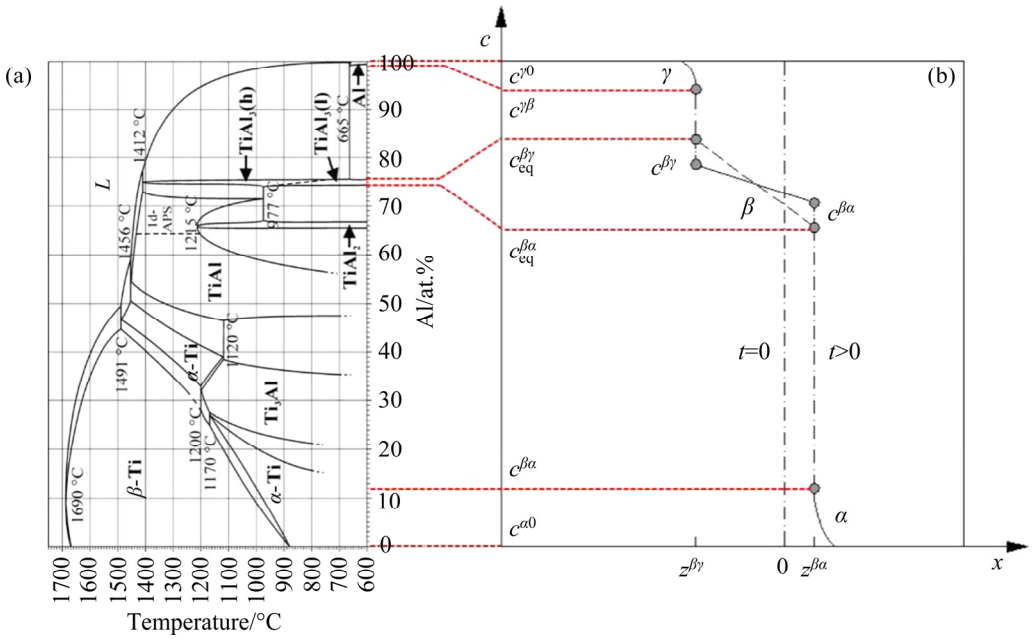

Fig. 9 Ti−Al binary alloy phase diagram [20] (a) and schematic diagram of Al concentration profile in α, β and γ phases (b)

compounds will not appear until the $TiAl_3$ phase grows to a particular thickness [26].

The $TiAl_3$ phase formation mechanism in cold-rolled laminated composites during annealing is described as follows. When the Ti/Al laminated composites are annealed at a given temperature T_0, the interdiffusion between Ti and Al occurs, the Al-rich and Ti-rich solid solution phases are generated. When the penetration depth of Ti in Al solid solution or Al in Ti solid solution reaches a nanometer-scale thickness, the $TiAl_3$ phase precipitates from the supersaturated solid solution and a continuous $TiAl_3$ layer is formed at the Ti/Al interface. The formation of the $TiAl_3$ phase obeys the following chemical reactions [27]:

$$\text{Ti(surface)+3Al(diffusing)=TiAl}_3 \quad (5)$$

$$\text{Ti(diffusing)+3Al(surface)=TiAl}_3 \quad (6)$$

With increasing the annealing time, the $TiAl_3$ phase thickens in the direction perpendicular to the Ti/Al interface. When the Ti/Al laminated composites are annealed for a particular time t, the Al concentration profiles across all phases along the diffusion direction are shown in Fig. 9(b). In this figure, the ordinate indicates the composition c of element Al; the abscissa shows the distance x; the vertical dot-dashed line at x=0 shows the initial position of the γ/α interface before annealing and the solid lines show the concentration profiles after annealing for a particular time; the variables α, β and γ represent the terminal solid solution phase of Ti(Al), $TiAl_3$ phase, and the terminal solid solution phase of Al(Ti), respectively; $z^{\beta\gamma}$ and $z^{\beta\alpha}$ indicate the migration distances of γ/β and β/α interfaces from the initial interface position after annealing, respectively; $c^{\gamma 0}$ and $c^{\alpha 0}$ are the initial concentrations of γ and α phases, respectively; $c^{\beta\gamma}$ and $c^{\gamma\beta}$ are the concentrations of β and γ phases at the γ/β interface, respectively; $c^{\alpha\beta}$ and $c^{\beta\alpha}$ are the concentrations of α and β phases at the α/β interface, respectively; $c_{\text{eq}}^{\beta\gamma}$ and $c_{\text{eq}}^{\beta\alpha}$ are the equilibrium concentrations of the β phase at the γ/β and α/β interfaces, respectively.

Because Al atoms hardly exist in Ti solid solution and Ti atoms hardly exist in Al solid solution, the diffusion fluxes in the α and γ phases are negligible. The α/β and γ/β interfaces can be considered as pure Al/$TiAl_3$ and Ti/$TiAl_3$ interfaces and symbols $c^{\alpha\beta}$ and $c^{\gamma\beta}$ can be replaced by $c^{\alpha 0}$ and $c^{\gamma 0}$, respectively. Furthermore, for simplicity, the interdiffusion coefficient D_β is assumed to be constant at the initial and second growth stages, which is reasonable because the $TiAl_3$ grain size increases very slowly with increasing annealing time. At the reaction-controlled growth stage, the relationship between the thickness of the $TiAl_3$ phase and annealing time can be expressed by the following equation [28]:

$$z^{\beta\alpha}-z^{\beta\gamma}=(K_{\beta\alpha}\frac{c-c_{\text{eq}}^{\beta\alpha}}{c-c^{\alpha 0}}+K_{\beta\gamma}\frac{c-c_{\text{eq}}^{\beta\gamma}}{c-c^{\gamma 0}})t=K_{\text{c}}t \quad (7)$$

where $K_{\beta\alpha}$ and $K_{\beta\gamma}$ are the reaction rate constants at the α/β and γ/β interfaces, respectively; the concentration c=$c^{\beta\alpha}$=$c^{\beta\gamma}$, and can be described by the following equation:

$$c=\frac{K_{\beta\alpha}c_{\text{eq}}^{\beta\alpha}+K_{\beta\gamma}c_{\text{eq}}^{\beta\gamma}}{K_{\beta\alpha}+K_{\beta\gamma}} \quad (8)$$

Equations (7) and (8) show that the growth rate is dominated by the chemical reaction rate constants $K_{\beta\alpha}$ and $K_{\beta\gamma}$. At the diffusion-controlled growth stage, the relationship between the thickness of the $TiAl_3$ phase and annealing time can be expressed by the following equation:

$$(z^{\beta\alpha}-z^{\beta\gamma})^2=2D_\beta(c_{\text{eq}}^{\beta\gamma}-c_{\text{eq}}^{\beta\alpha})\cdot(\frac{1}{c_{\text{eq}}^{\beta\alpha}-c^{\alpha 0}}-\frac{1}{c_{\text{eq}}^{\beta\gamma}-c^{\gamma 0}})t=K_{\text{d}}t \quad (9)$$

Equation (9) shows that the growth rate is dominated by the interdiffusion coefficient D_β because the values of $c^{\alpha 0}$, $c_{\text{eq}}^{\beta\gamma}$, $c_{\text{eq}}^{\beta\alpha}$ and $c^{\gamma 0}$ remain almost unchanged at different annealing temperatures.

In the above model, the concentration of Al is described in mol per unit volume. However, the molar fraction of Al (y) is used to express the composition of each phase in the Ti−Al binary alloy phase diagram. The molar fraction y can be converted into the concentration c by the equation c=y/V_{m}, where V_{m} is the molar volume of the relevant phase. The molar volumes of Ti, Al, and $TiAl_3$ are 10.6, 10.0, and 9.6 cm^3/mol, respectively [29]. Because the differences among the molar volumes of Ti, Al, and $TiAl_3$ are negligible, the molar concentrations $c^{\alpha 0}$, $c_{\text{eq}}^{\beta\gamma}$, $c_{\text{eq}}^{\beta\alpha}$, and $c^{\gamma 0}$ can be replaced with the molar fractions $y^{\alpha 0}$, $y_{\text{eq}}^{\beta\gamma}$, $y_{\text{eq}}^{\beta\alpha}$, and $y^{\gamma 0}$, respectively. In addition, the homogeneity range of the $TiAl_3$ phase ($\Delta y^\beta=y_{\text{eq}}^{\beta\gamma}-y_{\text{eq}}^{\beta\alpha}$) is narrow and roughly equal to 0.8 at.% [20], hence, Eq. (9) can be replaced by the

following equation:

$$(z^{\beta\alpha}-z^{\beta\gamma})^2=2D_\beta(y_{eq}^{\beta\gamma}-y_{eq}^{\beta\alpha})\cdot\frac{y^{\alpha0}-y^{\gamma0}}{(y^\beta-y^{\alpha0})(y^\beta-y^{\gamma0})}t=K_dt \quad (10)$$

where y^β represents the average Al molar fraction of the $TiAl_3$ phase.

3.4 Comparison and discussion on $TiAl_3$ phase growth kinetics in different studies

The experimental results of the growth kinetics of the $TiAl_3$ phase in different studies are summarized in Table 3. Except for the experimental results obtained by the present authors and FOADIAN et al [10], other studies found only the chemical reaction-controlled growth or diffusion-controlled growth for the $TiAl_3$ phase. This is mainly because other studies used different methods and raw materials to prepare the diffusion couple, which resulted in different critical time for the transition from the reaction-controlled growth to the diffusion-controlled growth. Moreover, they only conducted the experiment at one of the two growth stages. This also explains why only the chemical reaction-controlled growth mechanism of the $TiAl_3$ phase exists at 525 °C in the time range of 0−128 h in this work.

As shown in Table 3, the chemical reaction activation energy obtained in the present work (195.75 kJ/mol) is approximate to that obtained by LOO and RIECK (179.5 kJ/mol) [24], and less than that obtained by XU et al (295.8 kJ/mol) [22]. Figure 10 shows the relationships between the chemical reaction rate constant and annealing temperature obtained by different researchers. It can be seen from Fig. 10 that the reaction rate constants at different temperatures in the present work are much larger than those in other works, which can be attributed to different Ti/Al diffusion couple preparation methods. In this study, the Ti/Al diffusion couples were prepared by cold rolling, the oxide films of Ti and Al, which were mainly TiO_2 and Al_2O_3, were thin owing to the lower processing temperature, and Ti and Al were bonded with fresh surfaces because the pressure caused thin oxide films to disperse fully at the Ti/Al interface [30]. In contrast, XU et al [22] and LOO and RIECK [24] prepared the Ti/Al diffusion couples by diffusion welding and hot dipping, respectively, the thicker oxide films can be formed easily at the Ti/Al interface owing to the higher processing temperature. The oxide films can hinder the $TiAl_3$ phase nucleation at the interface [31]. Furthermore, it is difficult for Ti and Al atoms to diffuse through

Table 3 Comparison of $TiAl_3$ phase growth kinetics in different studies

Diffusion couple	Temperature/ °C	Time/ h★	n	K_{c0}/(m·s^{-1}) or K_{d0}/(m^2·s^{-1})▼	Q_c or Q_d/ (kJ·mol^{-1})	Source
99.6 wt.% Ti/99.5 wt.% Al	525−625	1/12−1	1	1.57×10^3	195.75	This work
99.6 wt.% Ti/99.0 wt.% Al	650	0.5−2	1	−	−	[7]
99.9 wt.% Ti/99.6 wt.% Al	570−630	1−12.8	0.63−0.93	1.47×10^4◆	232.1	[10]
99.5 wt.% Ti/99.5 wt.% Al	600−650	1−4	1	1.2×10^8	295.8	[22]
99.7 wt.% Ti/99.99 wt.% Al	580−640	2−20	1	3.95	179.50	[24]
99 wt.% Ti/99.9 wt.% Al	560−630	6−46	0.5	27.39▲	260.87▲	[13]
98.7 wt.% Ti/99.2 wt.% Al	500−630	1−25	0.5	3.5	237	[12]
98.0 wt.% Ti/9.99 wt.% Al	530−630	1−4	0.5	2.28×10^{-7}	105.1	[8]
TiAl/9.99 wt.% Al	516−640	2−25	0.5	1.30×10^{-7}	95.0	[24]
99.5 wt.% Ti/99.99 wt.% Al	540−650	4−64	0.5	1.96×10^{-11}▲	33.8	[15]
99.9 wt.% Ti/99.6 wt.% Al	570−630	12.8−260	0.31−0.56	−	17.4	[10]
99.6 wt.% Ti/99.5 wt.% Al	550−625	1−64	0.5	1.22×10^{-11}	33.69	This work

▼The symbol is K_{c0} when n=1, and K_{d0} when n=0.5. ★Because the annealing time is different at different annealing temperatures, the annealing time at the highest annealing temperature in these studies is adopted uniformly. ◆This value is recalculated using Eqs. (1) and (3) based on the reaction rate constants in the temperature range of 570−630 °C in Ref. [10]. ▲These values are recalculated using Eqs. (1) and (4) based on the $TiAl_3$ phase thicknesses in Refs. [13] and [15], respectively

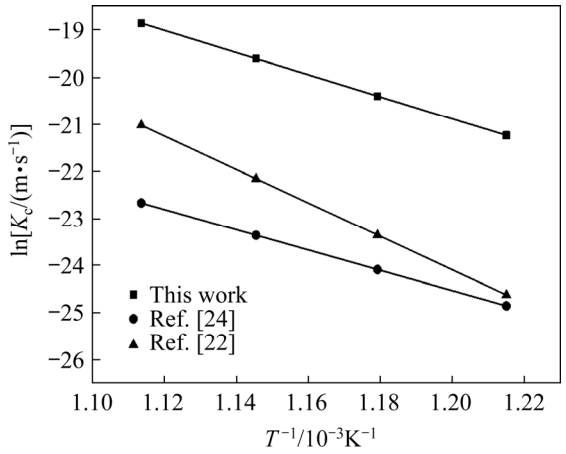

Fig. 10 Plot of ln K_c versus T^{-1} for $TiAl_3$ layer obtained by different researchers

the oxide films [32,33]. Therefore, the $TiAl_3$ phase growth in the experiments by XU et al [22] and LOO and RIECK [24] may be controlled by oxide films at the initial linear growth stage.

Some studies considered that the growth of the $TiAl_3$ phase is controlled by volume diffusion because the value of n is equal to 0.5. In fact, the value of n also equals 0.5 for the volume and grain boundary mixed diffusion-controlled growth when the grain size of the $TiAl_3$ phase remains unchanged with annealing time. If the annealing temperature is high and the time is long, the n value deviates from 0.5 because the grain size of the $TiAl_3$ phase increases gradually, which can be observed in the present work and the work of FOADIAN et al [10]. Furthermore, we note from Table 3 that the diffusion activation energies and diffusion growth rate constants in different studies vary significantly in the case of n=0.5, suggesting that the $TiAl_3$ phase growth is dominated by the volume and grain boundary mixed diffusion, or even grain boundary diffusion alone.

The diffusion growth rate constant K_d is not a material constant but varies with the compositions of the end-members of the diffusion couple [34]. Hence, it is necessary to convert the diffusion growth rate constants of the $TiAl_3$ phase in different studies to the effective diffusion coefficients of the $TiAl_3$ phase, and then compare these effective diffusion coefficients with each other. By rearranging Eq. (10), the effective diffusion coefficient of the polycrystalline $TiAl_3$ phase D_β can be obtained by the following equation:

$$D_\beta = \frac{(y^\beta - y^{\alpha 0})(y^{\gamma 0} - y^\beta)}{y^{\gamma 0} - y^{\alpha 0}} \frac{K_d}{2\Delta y^\beta} \tag{11}$$

Because the grain size of the $TiAl_3$ phase is on the micron or sub-micron scale and the ratio of the highest annealing temperature in this experiment (898 K) to the melting point of the $TiAl_3$ phase T_m (1613 K) is merely 0.56, both the volume and grain boundary diffusions in $TiAl_3$ phase should be considered in the present work [35]. The volume and grain boundary diffusion coefficients of the $TiAl_3$ phase can be expressed by the Arrhenius formula as follows, respectively [36]:

$$D_v = D_{v0} \exp[-Q_v/(RT)] \tag{12}$$

$$D_{gb} = D_{gb0} \exp[-Q_{gb}/(RT)] \tag{13}$$

where D_v and D_{gb} are the volume and grain boundary diffusion coefficients, respectively, m^2/s; D_{v0} and D_{gb0} are the pre-exponential factors, respectively, m^2/s; Q_v and Q_{gb} are the activation energies, respectively, kJ/mol. Usually $Q_{gb} \approx 0.5 Q_v$ for the face-centered cubic structure metals. The effective diffusion coefficient of the polycrystalline $TiAl_3$ phase D_β can be calculated as the combination of volume and grain boundary diffusion coefficients by the following equation [23]:

$$D_\beta = \frac{q\delta}{d} D_{gb} + D_v \tag{14}$$

where q is a numerical factor depending on the grain shape with q=3 for equiaxed grains and q=1 for columnar grains; δ is the grain boundary width, which is approximately equal to 0.5 nm; d is the grain size. D_β also follows the Arrhenius formula:

$$D_\beta = D_{\beta 0} \exp[-Q_\beta/(RT)] \tag{15}$$

where $D_{\beta 0}$ and Q_β are the pre-exponential factor and the effective diffusion activation energy, respectively.

Because $y^{\alpha 0}$, $y^{\gamma 0}$, y^β, and Δy^β remain unchanged in the temperature range of 525−625 °C, Eq. (11) shows that the effective diffusion coefficient D_β is proportional to the diffusion growth rate constant K_d and the diffusion growth activation energy Q_d is equal to the effective diffusion activation energy Q_β. In addition, it can be seen from Eqs. (11)−(15) that the effective diffusion activation energy Q_β and the effective diffusion coefficient D_β have different values due to different relative contributions of the

grain boundary diffusion coefficient D_{gb} and volume diffusion coefficient D_v. For instance, if $D_v \gg q\delta D_{gb}/d$ in the annealing temperature range, the $TiAl_3$ phase growth is governed by volume diffusion, the effective diffusion activation energy Q_β is approximate to the volume diffusion activation energy Q_v and the effective diffusion coefficient D_β is small. However, if $q\delta D_{gb}/d \gg D_v$ in the annealing temperature range, the growth of the $TiAl_3$ phase is governed by grain boundary diffusion, the effective diffusion coefficient D_β is large and the effective diffusion activation energy Q_β depends mainly on the grain boundary diffusion activation energy Q_{gb} and grain size d. For grain boundary diffusion, if d remains unchanged with the increase of annealing temperature, then $Q_\beta=Q_{gb}$; if d increases with increasing annealing temperature, then $Q_\beta<Q_{gb}$, and the larger the change of the grain size d with annealing temperature, the smaller the effective diffusion activation energy Q_β.

When the effective diffusion coefficient D_β is calculated from the data in Table 3, for simplicity, the Ti and Al alloys with different impurities in these diffusion couples are replaced by pure Ti and pure Al, respectively, and the Al molar fractions in the TiAl phase and $TiAl_3$ phase are set to be 0.5 and 0.75, respectively. The relationship between the calculated natural logarithm value of D_β and the reciprocal of temperature is shown in Fig. 11, which shows that the effective diffusion coefficients and effective diffusion activation energies of the $TiAl_3$ phase can be divided into two groups. The calculated results in Group I are obtained from the experiments in Refs. [12,13], which are characterized by a smaller effective diffusion coefficient and a larger effective diffusion activation energy. The calculated results in Group II are obtained from the experiments in Refs. [8,15,24] and this study, which are characterized by a larger effective diffusion coefficient and a smaller effective diffusion activation energy.

The tetragonal crystal structure of the $TiAl_3$(l) phase can be regarded as the deformed face-centered cubic structure of Al (a=0.4049 nm) with an elongation of 4.4% along the c direction and a contraction of 4.2% along the a and b directions, respectively. Similarly, the tetragonal crystal structure of the $TiAl_3$(h) phase can be regarded as the deformed face-centered cubic structure of Al with an elongation of 4.4% along the c direction

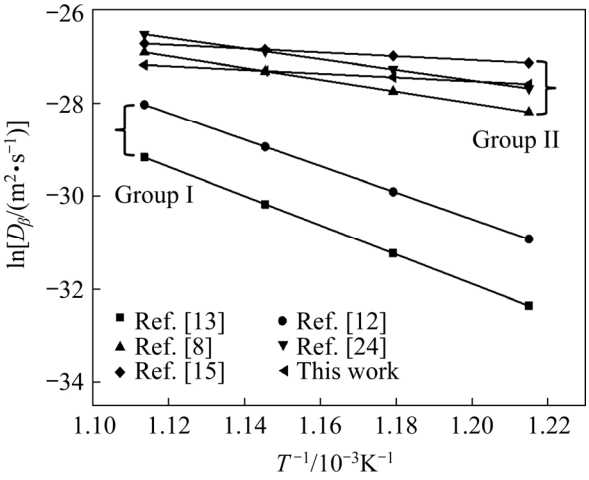

Fig. 11 Plot of ln D_β versus T^{-1}

and a contraction of 4.9% along the a and b directions, respectively. Hence, the volume diffusion in the $TiAl_3$ phase can be considered as the first-order approximation of diffusion in the close-packed face-centered cubic lattices. For the face-centered cubic metals self-diffusing via vacancy mechanism, the following empirical formula exists between the melting point T_m and the volume diffusion activation energy Q_v [29]:

$$\frac{Q_v}{T_m} \approx 146.5 \text{ J/K} \tag{16}$$

According to Eq. (16), the theoretical volume diffusion activation energy of the $TiAl_3$ phase is found to be 236.30 kJ/mol, which is very close to the diffusion growth activation energy obtained by NONAKA et al (237 kJ/mol) [12] and slightly smaller than that obtained by SUN et al (260.87 kJ/mol) [13]. Therefore, it can be inferred that the growth of the $TiAl_3$ phase is mainly controlled by volume diffusion in the experiments by NONAKA et al [12] and SUN et al [13].

It can be seen from Fig. 11 that the effective diffusion coefficients in Group II are approximate to each other in the temperature range of 550−625 °C, which are 64.1−184.5, 32.7−69.3, 17.4−27.6, and 9.2−14.0 times of those obtained by SUN et al [13] at 550, 575, 600, and 625 °C, respectively. At the diffusion-controlled growth stage, the effective diffusion coefficient and growth rate constant of the $TiAl_3$ phase can be affected by the impurity elements besides the shape and size of $TiAl_3$ grains. For example, NONAKA et al [12] found that the growth rate constant of $TiAl_3$ phase

in the Ti/Al diffusion couple with 5 at.% O on the Ti side is 0.41−0.56 times of that in the Ti/Al diffusion couple containing 0.35 at.% O on the Ti side. They considered that the aluminum oxide formed at the Al/$TiAl_3$ interface prevents the growth of the $TiAl_3$ phase. TARDY and TU [29] annealed the Ti/Al and Ti/(Al−0.25at.%Cu) diffusion couples at 400 °C for 3 h and found that the $TiAl_3$ layer thicknesses were 208 and 130 nm for Ti/Al and Ti/(Al−0.25at.%Cu) diffusion couples, respectively. They considered that the reason why the addition of 0.25 at.% Cu to Al retarded the diffusion-controlled growth of the $TiAl_3$ phase is that the higher activation energy is needed to break Ti atoms away from Cu atoms owing to the strong binding energy between Ti and Cu atoms. The Ti/Al diffusion couple prepared by SUN et al [13] has 0.63 wt.% Si and 0.18 wt.% O (0.54 at.%) on the Ti side and 0.096 wt.% Si and 0.21 wt.% O (0.63 at.%) on the Al side. The Ti/Al diffusion couple prepared by NONAKA et al [12] has 0.2 wt.% Mg, 0.15 wt.% Fe, 0.27 wt.% Si and 0.11 wt.% Mn on the Al side, and 0.047 wt.% Fe and 0.117 wt.% O (0.35 at.%) on the Ti side. There is little oxygen on the Ti and Al sides of both the Ti/Al diffusion couples prepared by SUN et al [13] and NONAKA et al [12]. In addition, the contents of oxygen in the Ti/Al diffusion couples in Group II are close to those in Group I, so the differences in oxygen content could not account for the effective diffusion coefficients in Group II being much larger than those in Group I. A small amount of other impurity elements in the Ti/Al diffusion couples have also little effect on the effective diffusion coefficient of the $TiAl_3$ phase because the atomic radius and electronegativity of these impurity elements are approximate to those of Al and Ti, which was confirmed by previous studies [15,24]. Based on the above analysis, we concluded the fact that the effective diffusion coefficients in Group II are much larger than those in Group I can be mainly attributed to the growth of the $TiAl_3$ phase in Group II being dominated by grain boundary diffusion.

The effective diffusion activation energies obtained by SHIMOZAKI et al [15] and this study were 33.8 and 33.69 kJ/mol, respectively, which are much smaller than the theoretical grain boundary diffusion coefficient Q_{gb} (118.15 kJ/mol in the case of $Q_{gb}=0.5Q_v$). SHIMOZAKI et al [15] suggested that the low growth activation energy was due to two possible growth mechanisms of the $TiAl_3$ phase in the annealing temperature range of 540−650 °C. One is grain boundary diffusion- controlled growth at high temperature, and the other is oxide film-controlled growth at low temperature. However, in the present study, the influence of the oxide films was eliminated as Ti and Al were bonded with fresh surfaces. Therefore, we believed that the growth of the $TiAl_3$ phase is mainly controlled by grain boundary diffusion during annealing at 525−625 °C. We further suggested that the low effective diffusion activation energy is caused by the grain size increase of the $TiAl_3$ phase with an increase of annealing temperature, which causes the negative effect from the growth of $TiAl_3$ grains partly counteracting the positive effect from annealing temperature on the diffusion coefficient of the $TiAl_3$ phase. The effective diffusion activation energies obtained by KRÁĹ et al [8] and LOO and RIECH [24] are 105.1 and 95.0 kJ/mol, respectively, which are approximate to the theoretical grain boundary diffusion energy of the $TiAl_3$ phase and could be attributed to the smaller change in grain size with increasing annealing temperature.

4 Conclusions

(1) Only one intermetallic compound $TiAl_3$ phase is formed at the Ti/Al interface, and the $TiAl_3$ phase exhibits fine equiaxed grains with average sizes ranging from a few hundred nanometers to a few microns. The average grain size of the $TiAl_3$ phase increases with the increase of annealing temperature and/or annealing time, but the effect of annealing temperature on the average grain size is far greater than that of annealing time.

(2) The $TiAl_3$ phase growth can be divided into two stages. At the initial annealing stage, n=1.0, the $TiAl_3$ phase growth is governed by chemical reaction with a reaction activation energy of 195.75 kJ/mol. At the second stage, n=0.5, the growth of the $TiAl_3$ phase is governed by diffusion with a diffusion growth activation energy of 33.69 kJ/mol. The higher the annealing temperature, the smaller the critical thickness corresponding to the transition from chemical reaction-controlled growth to diffusion-controlled growth.

(3) At the reaction-controlled growth stage, since Ti and Al are bonded with fresh surfaces, the

chemical reaction rate constant of the $TiAl_3$ phase in Ti/Al laminated composites prepared by cold rolling is far larger than those prepared by other methods in which oxide films exist at the Ti/Al interface. At the diffusion-controlled growth stage, the growth of the $TiAl_3$ phase is determined by the effective diffusion coefficient of the $TiAl_3$ phase which is mainly attributed to the grain boundary diffusion owing to the smaller $TiAl_3$ grain size.

Acknowledgments

The authors are grateful for the financial supports from the S&T Program of Hebei Province, China (No. 20373901D), the National Natural Science Foundation of China (Nos. 51807047, 51804095), the National Science Foundation of Hebei Province, China (No. E2019402433), the Youth Top Talents Science and Technology Research Project of Hebei Province University, China (No. BJ2019003), and the Research and Development Project of Science and Technology of Handan City, China (No. 19422111008-19).

References

[1] FAN Xue-lin, YUAN Mei-ni, QIN Qiang. Failure mechanisms of Ti−Al_3Ti metal−intermetallic laminate composites under high-speed impact [J]. Rare Metal Materials and Engineering, 2018, 47: 2615−2620.

[2] ASSARI A H, EGHBALI B. Solid state diffusion bonding characteristics at the interfaces of Ti and Al layers [J]. Journal of Alloys and Compounds, 2019, 773: 50−58.

[3] CUI Xi-ping, FAN Guo-hua, GENG Lin, WANG Yin, HUANG Lu-jun, PENG Hua-xin. Growth kinetics of $TiAl_3$ layer in multi-laminated Ti−(TiB_2/Al) composite sheets during annealing treatment [J]. Materials Science and Engineering A, 2012, 539: 337−343.

[4] ZHANG Jun-peng, HUANG Hua-gui, ZHAO Ri-dong, FENG Miao, MENG Kai. Cast-rolling force model in solid−liquid cast-rolling bonding (SLCRB) process for fabricating bimetal clad strips [J]. Transactions of Nonferrous Metals Society of China, 2021, 31: 626−635.

[5] LAZURENKO D V, BATAEV I A, MALI V I, BATAEV A A, MALIUTINA I N, LOZHKIN V S, ESIKOV M A, JORGE A M J. Explosively welded multilayer Ti−Al composites: Structure and transformation during heat treatment [J]. Materials and Design, 2016, 102: 122−130.

[6] ESTHER I, DINAHARAN I, MURUGAN N. Microstructure and wear characterization of AA2124/4wt.%B_4C nano-composite coating on Ti−6Al−4V alloy using friction surfacing [J]. Transactions of Nonferrous Metals Society of China, 2019, 29: 1263−1274.

[7] LUO J G, ACOFF V L. Using cold roll bonding and annealing to process Ti/Al multi-layered composites from elemental foils [J]. Materials Science and Engineering A, 2004, 379: 164−172.

[8] KRÁĹ J, FERDINANDY M, LIŠKA D, DIKO P. Formation of $TiAl_3$ layer on titanium alloys [J]. Materials Science and Engineering A, 1991, 140: 479−485.

[9] FRONCZEK D M, WOJEWODA-BUDKA J, CHULIST R, SYPIEN A, KORNEVA A, SZULC Z, SCHELL N, ZIEBA P. Structural properties of Ti/Al clads manufactured by explosive welding and annealing [J]. Materials and Design, 2016, 91: 80−89.

[10] FOADIAN F, SOLTANIEH M, ADELL M, ETMINAN-BAKHSH M. The kinetics of $TiAl_3$ formation in explosively welded Ti−Al multilayers during heat treatment [J]. Metallurgical and Materials Transactions B, 2016, 47: 2931−2937.

[11] FRONCZEK D M, CHULIST R, LITYNSKA-DOBRZYNSKA L, SZULC Z, ZIEBA P, WOJEWODA-BUDKA J. Microstructure changes and phase growth occurring at the interface of the Al/Ti explosively welded and annealed joints [J]. Journal of Materials Engineering and Performance, 2016, 25: 3211−3217.

[12] NONAKA K, FUJII H, NAKAJIMA H. Effect of oxygen in titanium on reaction diffusion between Ti and Al [J]. Materials Transactions, 2001, 42: 1731−1740.

[13] SUN Yu. WAN Zhi-peng, HU Lian-xi, WU Bing-hua, DENG Tai-qing. Characterization on solid phase diffusion reaction behavior and diffusion reaction kinetic of Ti/Al [J]. Rare Metal Materials and Engineering, 2017, 46: 2080−2086.

[14] MIRJALILI M, SOLTANIEH M, MATSUURA K, OHNO M. On the kinetics of $TiAl_3$ intermetallic layer formation in the titanium and aluminum diffusion couple [J]. Intermetallics, 2013, 32: 297−302.

[15] SHIMOZAKI T, OKINO T, YAMANE M, WAKAMATSU Y, ONISHI M. Effect of diffusion barrier and impurities in titanium on the growth rate of $TiAl_3$ layer [J]. Defect and Diffusion Forum, 1997, 143−147: 591−596.

[16] DU Y, CHANG Y A, HUANG B Y, GONG W P, JIN Z P, XU H H, YUAN Z H, LIU Y, HE Y H, XIE F Y. Diffusion coefficients of some solutes in fcc and liquid Al: Critical evaluation and correlation [J]. Materials and Science Engineering A, 2003, 363: 140−151.

[17] ARAÚJO L L, BEHAR M. Al and Ag diffusion study in α-titanium [J]. Applied Physics A, 2000, 71: 169−174.

[18] SCHUSTER J C, PALM M. Reassessment of the binary aluminum−titanium phase diagram [J]. Journal of Phase Equilibria and Diffusion, 2006, 27: 255−277.

[19] RAO V B, HOUSKA C R. Reactions and diffusion between an Al film and a Ti substrate [J]. Metallurgical Transactions A, 1983, 14: 61−66.

[20] OKAMOTO H. Al−Ti (aluminum−titanium) [J]. Journal of Phase Equilibria, 1993, 14: 120−121.

[21] THIYANESHWARAN N, SIVAPRASAD K, RAVISANKAR B. Nucleation and growth of $TiAl_3$ intermetallic phase in diffusion bonded Ti/Al metal intermetallic laminate [J]. Scientific Reports, 2018, 8: 16797.

[22] XU L, CUI Y Y, HAO Y L, YANG R. Growth of intermetallic layer in multi-laminated Ti/Al diffusion couples

[J]. Materials Science and Engineering A, 2006, 435/436: 638−647.
[23] FURUTO A, KAJIHARA M. Numerical analysis for kinetics of reactive diffusion controlled by boundary and volume diffusion in a hypothetical binary system [J]. Materials Transactions, 2008, 49: 294−303.
[24] van LOO F J J, RIECK G D. Diffusion in the titanium−aluminum system—I. Interdiffusion between solid Al and Ti or Ti−Al alloys [J]. Acta Metallurgica, 1973, 21: 61−71.
[25] LIU Jiang-ping, SU Yan-ying, XU Yan-jin, LUO Liang-shun, GUO Jing-jie, FU Heng-zhi. First phase selection in solid Ti/Al diffusion couple [J]. Rare Metal Materials and Engineering, 2011, 40: 753−756.
[26] WÖHLERT S, BORMANN R. Phase selection governed by different growth velocities in the early stages of the Ti/Al phase reaction [J]. Journal of Applied Physics, 1998, 85: 825−832.
[27] DYBKOV V I. Reaction diffusion in heterogeneous binary systems [J]. Journal of Materials Science, 1986, 21: 3078−3084.
[28] BALLUFFI R W, ALLEN S M, CARTER W C. Kinetics of materials [M]. New Jersey: John Wiley & Sons, Inc., 2005.
[29] TARDY J, TU K N. Solute effect of Cu on interdiffusion in Al_3Ti compound films [J]. Physical Review B, 1985, 32: 2070−2081.
[30] LI L, NAGAI K, YIN F. Progress in cold roll bonding of metals [J]. Science and Technology of Advanced Materials, 2008, 9: 023001.
[31] THUILLARD M, TRAN L T, NICOLET M A. Al_3Ti formation by diffusion of aluminum through titanium [J]. Thin Solid Films, 1988, 166: 21−28.
[32] ZHANG Q, XIAO B L, WANG W G, MA Z Y. Reactive mechanism and mechanical properties of in situ composites fabricated from an Al−TiO_2 system by friction stir processing [J]. Acta Materialia, 2012, 60: 7090−7103.
[33] HARACH D J, VECCHIO K S. Microstructure evolution in metal−intermetallic laminate (MIL) composites synthesized by reactive foil sintering in air [J]. Metallurgical and Materials Transactions A, 2001, 32: 1493−1505.
[34] PAUL A, LAURILA T, VUORINEN V, DIVINSKI S V. Thermodynamics, diffusion and the Kirkendall effect in solids [M]. Cham: Springer International Publishing, 2014.
[35] PORTER D A, EASTERLING K E, SHERIF M Y. Phase transformations in metals and alloys [M]. 3rd ed. Boca Raton: CRC Press, 1992.
[36] MISHIN Y, HERZIG C. Grain boundary diffusion: Recent progress and future research [J]. Materials Science and Engineering A, 1999, 260: 55−71.

冷轧 Ti/Al 层状复合材料中 $TiAl_3$ 相在退火过程中的形成机理及生长动力学

张建宇[1,2]，王艳辉[1,2]，吕 征[1,2]，陈庆安[1,2]，陈亚宇[1,2]，李河宗[1,2]

1. 河北工程大学 机械与装备工程学院，邯郸 056038；
2. 河北工程大学 河北省智能工业装备技术重点实验室，邯郸 056038

摘 要：将冷轧 Ti/Al 层状复合材料在 525~625 °C 温度范围内退火 0~128 h，并对复合材料的界面显微组织演变进行研究。结果表明，仅金属间化合物 $TiAl_3$ 相在 Ti/Al 界面形成，大多数 $TiAl_3$ 晶粒为细小的等轴晶，其平均尺寸从数百纳米到数微米，且随温度和/或退火时间的增加而增加，其中退火温度对晶粒尺寸的影响远大于退火时间的影响。$TiAl_3$ 相的生长可分为两个阶段：在初始阶段，$TiAl_3$ 相的生长由化学反应控制，反应激活能为 195.75 kJ/mol，另外，由于冷轧方法制备的 Ti/Al 层状复合材料的界面与新鲜表面结合，$TiAl_3$ 相的反应速率常数较大；在第二阶段，$TiAl_3$ 相的生长由扩散控制，扩散激活能为 33.69 kJ/mol，另外，由于 $TiAl_3$ 相晶粒尺寸细小，$TiAl_3$ 相的扩散生长速率常数由晶界扩散决定。

关键词：Ti/Al 层状复合材料；退火；生长动力学；$TiAl_3$ 相；形成机理

(Edited by Wei-ping CHEN)